GFZ
Helmholtz-Zentrum
POTSDAM

Originally published as:

Vinnik, L. P., Oreshin, S. I., Speziale, S., Weber, M. (2010): Mid-mantle layering from SKS receiver functions. - Geophysical Research Letters, 37, L24302

DOI: 10.1029/2010GL045323

Mid-mantle layering from SKS receiver functions

L. P. Vinnik,[1] S. I. Oreshin,[1] S. Speziale,[2] and M. Weber[2,3]

Received 30 August 2010; revised 12 October 2010; accepted 19 October 2010; published 18 December 2010.

[1] Many seismic data on mid-mantle discontinuities are related only to subduction zones. Here we use a method that is applicable outside subduction zones. The idea is to use SKS-to-P converted phases that are generated in the receiver regions and can be detected in S receiver functions. In two regions (southern Africa and Western Europe) we have detected apparently the same '1200-km' discontinuity, but at a depth that varies from 1170 km (Africa) to 1240–1270 km (Europe). The S velocity contrast at this discontinuity is ~0.1 km/s, i.e., half of the value in subduction zones. The '1200-km' discontinuity may correspond to the phase transition of SiO_2 from stishovite to $CaCl_2$ structure. The small S velocity contrast is compatible with scenarios in which small remnants of old subducted oceanic lithosphere, thermally equilibrated and partly reacted, are finely dispersed in a bulk mantle matrix. **Citation:** Vinnik, L. P., S. I. Oreshin, S. Speziale, and M. Weber (2010), Mid-mantle layering from SKS receiver functions, *Geophys. Res. Lett.*, *37*, L24302, doi:10.1029/2010GL045323.

1. Introduction

[2] Seismic discontinuities inside the Earth are of interest because they present signatures of phase transitions, or of compositional layering. Reports on lower-mantle layering are known since the early days of seismology [*Wiechert and Zoeppritz*, 1907]. In the late sixties, indications of lower-mantle discontinuities were found in results of direct measurements of P-wave slowness at large-aperture seismograph arrays [e.g., *Chinnery*, 1969; *Johnson*, 1969; *Vinnik and Nikolayev*, 1970]. More recently observations of short-period (~1 s) seismic waves converted from S to P in source regions proved to be very informative on discontinuities at depths between about 900 km and 1500 km [e.g., *Bock and Ha*, 1984; *Wicks and Richards*, 1993; *Kawakatsu and Niu*, 1994; *Niu and Kawakatsu*, 1997; *Vanacore et al*., 2006]. These observations require recordings of deep earthquakes, and the cited results are characteristic of subduction zones of the west Pacific.

[3] Discontinuities with a width of more than a few kilometers are transparent for S waves with a period of ~1 s, but converted phases of significant amplitude can be observed at longer periods. *Vinnik et al.* [1998, 2001] detected these phases in recordings of a number of deep events in the western Pacific at a period of ~10 s. These observations generally confirmed the shorter-period data and revealed new details. Specifically, the clearest signals were obtained from a discontinuity in a depth range from 1170 to 1250 km in the Fiji-Tonga and Japan regions. Numerical modeling suggested that the S-velocity contrast at this discontinuity is ~0.2 km/s.

[4] Here we describe the method that does not require deep events and, for this reason, is applicable practically everywhere. We apply it in two regions outside Cenozoic subduction zones. The idea is to use S-to-P converted phases that are converted not in the source but in the receiver regions. They can be detected with a method similar to the S receiver function (SRF) technique [*Farra and Vinnik*, 2000]. This technique was used in the studies of the lithosphere/asthenosphere system and the transition zone [e.g., *Vinnik et al.*, 2009], but, as will be shown, it has a potential for the mid-mantle, as well. The other useful data on the mid-mantle discontinuities are underside SH and P reflections that can be detected as precursors to the SS [e.g., *An et al.*, 2007] and P'P' phases [e.g., *LeStunff et al.*, 1995], ScS reverberations [*Courtier and Revenaugh*, 2008] and P-to-S converted phases in P receiver functions [e.g., *Shen et al.*, 2003].

2. SKS Receiver Functions

[5] S receiver function (SRF) consists mostly of Sp converted phases (converted from S to P in the receiver region). The standard SRF technique is not suitable for the lower-mantle Sp phases owing to the large S wave slowness (more than ~9 s/°). The appropriate slowness range is provided only by the SKS phase. Therefore, we, first separate S and SKS wave fields in the recordings of each earthquake by space-time filtering at the receiver array, and then calculate SKS receiver functions, as described by *Vinnik et al.* [2009]. The slowness of the SKSp phases in a laterally homogeneous Earth is larger than the slowness of SKS. Therefore the individual receiver functions are stacked with move-out time corrections. The correction is calculated as product of the trial differential slowness and the differential epicentral distance.

[6] We apply two methods of stacking. In the first (linear) method the individual receiver functions are stacked with weights that are inversely proportional to the mean square amplitudes of seismic noise [*Farra and Vinnik*, 2000]. The second (non-linear) method is N-th-root stacking [*Muirhead*, 1968]. In this method, instead of the initial trace, the N-th root of it is taken, and the stack is then raised to the N-th power. The signal/noise ratio in the Nth-root stack can be enhanced relative to the linear stack. N = 2 provides a compromise between the nonlinear distortion of the waveforms and the gain in the signal/noise ratio.

3. Seismic Data

[7] The method was applied to two large seismograph arrays: SASE in southern Africa and the German Regional Seismograph Network (GRSN) (Figure 1). SASE (South

[1]Institute of Physics of the Earth, Moscow, Russia.
[2]Deutsches GeoForschungsZentrum, Potsdam, Germany.
[3]Institut für Geowissenschaften, Universität Potsdam, Potsdam, Germany.

Copyright 2010 by the American Geophysical Union.
0094-8276/10/2010GL045323

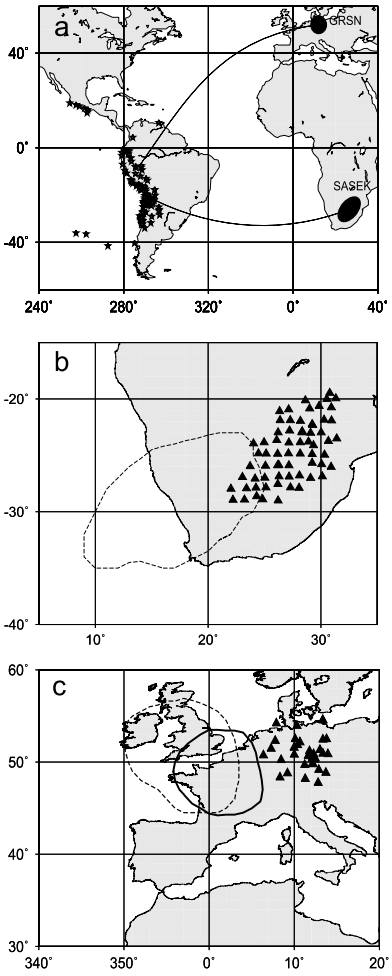

Figure 1. Source and receivers of this study. (a) Earthquake epicenters (stars) and GRSN and SASE arrays, (b) seismograph stations of the SASE array (triangles) and the region of piercing points at a depth of 1200 km (dashed line); (c) seismograph stations of the GRSN network and the regions of piercing points for the first (dashed line) and second (bold line) groups of events, respectively.

African Seismic Experiment) broad-band array was designed to study deep structure of southern Africa [*Carlson et al.*, 1996]. At SASE, we used recordings of 30 seismic events (both shallow and deep) in South America from 50 stations with the lowest noise (Figure 1b). The average epicentral distance is 89.5° which is suitable for detecting the converted phases from depths up to ~1400 km. For our sign convention, a positive discontinuity (with the higher S velocity at the lower side) corresponds to the downward motion in the receiver function. In the SASE stack (Figure 2) strong SKS660p and SKS410p phases can be observed. The only signal from the mid-mantle is at a time of −108.6 s. Its amplitude in the linear stack (Figure 2a) is 3 times the RMS value of noise, and a better signal/noise ratio is obtained by applying N-th-root technique (Figure 2b). From the previous analysis of the SASE recordings [*Vinnik et al.*, 2009] we know that the arrivals of the mantle Sp phases are delayed with respect to the standard IASP91 travel times [*Kennett and Engdahl*, 1991] by ~2.0 s. This is an effect of the anomalously low Vp/Vs ratio in the uppermost mantle of the Kalahari craton. With the allowance for this anomaly, the time of the mid-mantle Sp phase is −110.6 s, and the corresponding depth of the discontinuity is 1170 km. This time is measured with the uncertainty of ±0.5 s, and the uncertainty of the depth estimates is within ±10 km. The theoretical differential slowness of the SKS1170p phase is 0.7 s/°. The largest amplitude of this phase in the actual stack is at a slowness near the theoretical value (0.8 s/°). The piercing points of SKS1170p (cross-over of the ray-paths and the 1170-km discontinuity) are located beneath the western margin of the Kalahari craton and the southern Atlantic outlined by the dashed box (Figure 1).

[8] The GRSN network consists of nearly 30 stations (Figure 1). We processed 96 recordings of events of 1994–2008 from South America. The epicentral distances with respect to the center of the array are in the interval from 88° to 110° with an average of 99.5°, much larger than in southern Africa. The differential slowness of the SKSp phases from the mid-mantle varies from ~0.7 s/° at a distance of ~90° to ~0.3 s/° at a distance of ~100° and more. Therefore we divided the seismic events into two groups with a distance range from 88° to 100° (average of 95.4°) and from 100° to 110° (average of 104.6°). Both SKS660p and SKS410p are prominent phases in Figure 3a. The only clear signal from the mid-mantle is detected in both distance intervals (Figures 3a and 3b) at a time of ~114 s. The largest amplitude of this signal in the first distance interval (Figure 3a) is at a differential slowness of ~0.1 s/°, quite different from the

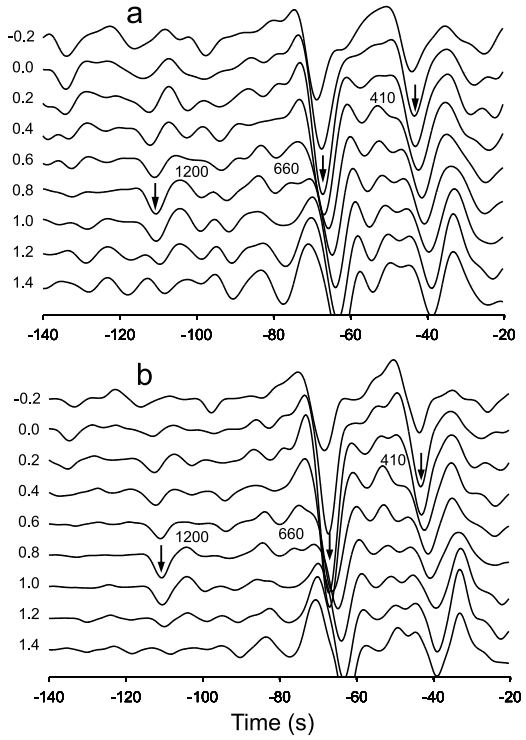

Figure 2. Stacks of the receiver functions of the SASE array. (a) Linear stack. (b) N-th-root stack. Each trace corresponds to the differential slowness shown on the left-hand side. Time is relative to SKS arrival. The detected phases are marked at the traces with the largest amplitudes.

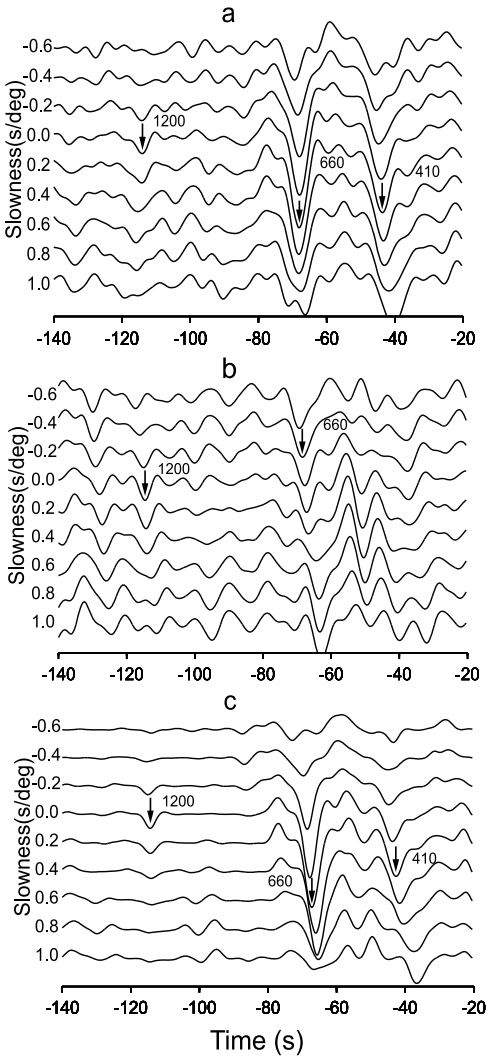

Figure 3. Stacks of the receiver functions of the GRSN network. (a) As Figure 2a, but for the first group of events. (b) As Figure 3a, but for the second group. (c) As Figure 2b but for all events.

theoretical value for the horizontal discontinuity (~0.7 s/°). This discrepancy could be caused by the converting interface that dips eastward with the angle of a few degrees. In the second distance interval (Figure 3b) the largest amplitude is again at a differential slowness of ~0.1 s/°, which for this distance range is close to the theoretical value for the horizontal interface (~0.3 s/°). In spite of the similar arrival times in the first and second intervals, the difference in the reference distance leads to different depths: 1240 km and 1270 km, respectively. The piercing points corresponding to the second interval are shifted eastward relative to the first interval (Figure 1), and the larger depth for the second group is consistent with the observed anomaly of the differential slowness.

[9] Assuming the existence of topography on the converting discontinuity the difference in the differential slowness between the two distance intervals is negligible, and all recordings can be processed together. The amplitude of the resulting signal in the linear stack is ~4 times the RMS value of noise, and an even higher signal/noise ratio is obtained by N-th-root stacking (Figure 3c). The resulting average depth of the converting interface is 1260 km.

4. Discussion

[10] We have detected apparently the same '1200-km' discontinuity in two regions, but at a variable depth. Our data for southern Africa are broadly consistent with the observations of precursors to the P'P' phase at seismograph stations in California [*LeStunff et al.*, 1995] with the bouncing points in a neighboring region of Africa. Apparently the same discontinuity was detected in subduction zones of the western Pacific [*Vinnik et al.*, 2001]. An estimate of the S velocity contrast at this discontinuity was 0.2 km/s. Comparable or larger estimates of the impedance of the mid-mantle discontinuities in subduction zones are reported elsewhere [*Courtier and Revenaugh*, 2008]. In our data the amplitude of the signal from this discontinuity is around a quarter of that from the 660-km discontinuity, and, accordingly, the contrast of the S velocity is ~0.09 km/s or ~1.5%. This estimate suggests that the '1200-km' discontinuity in subduction zones is larger than outside, but the data still are too few to conclude this with confidence.

[11] Previously discussed explanations of the mid-mantle discontinuities include remnants of subducted oceanic lithosphere, compositional stratification and effects of hydration. No phase transitions in the main mineral phases in this depth range are predicted for pyrolite [*Murakami et al.*, 2005; *Ono et al.*, 2005]. Our favorite explanation is the phase transition of SiO_2 from stishovite to $CaCl_2$ structure [*Tsuchida and Yagi*, 1989; *Kingma et al.*, 1995]. This phase transition is characterized by an unusual dependence of the S velocity on depth. The shear acoustic velocity along $\langle 110 \rangle$ vanishes before the transition, producing a low average S velocity and extreme elastic anisotropy [*Karki et al.*, 1997; *Carpenter et al.*, 2000]. The existing computational and experimental studies [*Karki et al.*, 1997; *Lakshtanov et al.*, 2007; *Jiang et al.*, 2009] show that the softening takes place across a broad depth range (on the order of a few hundred kilometers), whereas the recovery within the stability field of the post-stishovite phase is several times faster. The Sp converted phase can arise at the gradational boundary, only if the width of this boundary is not larger than the wavelength of the S wave, in our case 60 km or 3 GPa in pressure. This means that seismic detection of the stishovite softening in our data is unlikely. Moreover, this effect can be masked by the positive depth dependence of S velocity in other mantle minerals. The chances to detect the following velocity increase are certainly much better. We note that most of the usually cited seismic studies of mid-mantle discontinuities were conducted at the wavelengths of several kilometers, and a detection of the stishovite softening in this range is less likely than in our work. Moreover some of these studies were conducted with reflected phases. For them the limiting width of the gradational boundary is around a quarter of the wavelength.

[12] Lateral variations of depth of the discontinuity investigated in this study can be explained by the sensitivity of the depth to the concentration of Al_2O_3 [*Lakshtanov*

[1] Auxiliary materials are available in the HTML. doi:10.1029/2010GL045323.

et al., 2007]: the variations of depth in a range of 100 km require variations of Al_2O_3 in a range of 1 wt%. In subduction zones basalt in lower-mantle conditions transforms into a perovskite assemblage with about 10–20% of stishovite [*Hirose et al.*, 1999; *Kesson et al.*, 2002]. However, the presence of SiO_2 in the regions outside the subduction zones poses a problem. We postulate persistence in the mid-mantle of small (several kilometers) remnants of very old (Paleozoic?) subducted lithosphere. They would be thermally equilibrated and partially reacted [*Bina*, 2003, 2010]. Due to the partial reaction with the surrounding mantle, the proportion of SiO_2 in the original basalt/gabbro material would be reduced, and this would lead to a smaller seismic signal. The data on pure and Al-containing SiO_2 [*Cohen*, 1992; *Karki et al.*, 1997; *Tsuchiya et al.*, 2004; *Lakshtanov et al.*, 2007; *Nomura et al.*, 2010] suggest that the presence of 10 to 15 vol.% SiO_2 with 3 to 4 wt% Al_2O_3 would explain the discontinuity with a shear velocity contrast of 1.8%, consistent with our observations. Volume fractions of the order of 85% of MORB-like material and 15% of pyrolite would produce a discontinuity compatible with the present observations.

[13] Another possible effect at a depth of ~1200 km is a change in the Fe/Mg partition between mantle minerals. Recent experiments document a maximum in the Fe/Mg partition between Mg-rich perovskite and ferropericlase in pyrolite at pressures corresponding to the mid-mantle [*Irifune et al.*, 2010]. The maximum between 25 and 30 GPa is followed by a rapid decrease of this ratio in perovskite at around 40 GPa. A conservative estimate of Fe/Mg partitioning and Fe-spin transition in ferropericlase, including temperature effects calculated from the presently available data, suggest a flattening in the depth dependence of the S velocity of pyrolite followed by a rapid increase of S velocity of 0.5% between 1100 and 1200 km. This effect is weak relative to the required ~1.5%, but it can contribute to the observed seismic discontinuity. The details of our calculations are presented in the auxiliary materials.[1]

[14] **Acknowledgments.** The Russian team was supported by the grant 07-05-00315 from the Russian Fund for Basic Research (RFBR). L. Vinnik was also supported by the grant from Alexander-von-Humboldt foundation. We thank Klaus Stammler for his great help with the GRSN recordings. The recordings of the SASE array were obtained from IRIS DMC.

References

An, Y., Y. J. Gu, and M. D. Sacchi (2007), Imaging mantle discontinuities using least squares Radon transform, *J. Geophys. Res.*, *112*, B10303, doi:10.1029/2007JB005009.

Bina, C. R. (2003), Seismological constraints upon mantle composition, in *Treatise on Geochemistry*, vol. 2, *The Mantle and Core*, edited by R. Carlson, pp. 39–59, Elsevier, Amsterdam.

Bina, C. R. (2010), Scale limits of free-silica seismic scatterers in the lower mantle, *Phys. Earth Planet. Inter.*, doi:10.1016/j.pepi.2010.06.008, in press.

Bock, G., and J. Ha (1984), Short-period S-P conversions in the mantle at a depth near 700 km, *Geophys. J. R. Astron. Soc.*, *77*, 593–615.

Carlson, R. W., T. L. Grove, M. J. De Wit, and J. J. Gurney (1996), Program to study the crust and mantle of the Archean craton in Southern Africa, *Eos Trans. AGU*, *77*(29), 273, doi:10.1029/96EO00194.

Carpenter, M. A., R. J. Hemley, and H.-K. Mao (2000), High-pressure elasticity of stishovite and the $P4_2/mnm \leftrightarrow Pnnm$ phase transition, *J. Geophys. Res.*, *105*, 10,807–10,816.

Chinnery, M. A. (1969), Velocity anomalies in the lower mantle, *Phys. Earth Planet. Inter.*, *2*, 1–10, doi:10.1016/0031-9201(69)90013-2.

Cohen, R. E. (1992), First-principles prediction of elasticity and phase transitions in high-pressure SiO_2 and geophysical implications, in *High Pressure Research*, edited by Y. Syono and M. H. Manghnani, pp. 425–431, Terrapub, Tokyo.

Courtier, A. M., and J. Revenaugh (2008), Slabs and shear wave reflectors in the mid-mantle, *J. Geophys. Res.*, *113*, B08312, doi:10.1029/2007JB005261.

Farra, V., and L. P. Vinnik (2000), Upper mantle stratification by P and S receiver functions, *Geophys. J. Int.*, *141*, 699–712, doi:10.1046/j.1365-246x.2000.00118.x.

Hirose, K., Y. Fei, Y. Ma, and H.-K. Mão (1999), The fate of subducted basaltic crust in the Earth's lower mantle, *Nature*, *397*, 55–56.

Irifune, T., T. Shinmei, C. A. McCammon, M. Myajima, D. C. Rubie, and D. J. Frost (2010), Iron partitioning and density changes of pyrolite in Earth's lower mantle, *Science*, *327*, 193–195, doi:10.1126/science.1181443.

Jiang, F., G. D. Gwanmesia, T. I. Dyuzheva, and T. S. Duffy (2009), Elasticity of stishovite and acoustic mode softening under high pressure by Brillouin scattering, *Phys. Earth Planet. Inter.*, *172*, 235–240.

Johnson, L. R. (1969), Array measurements of P velocities in the lower mantle, *Bull. Seismol. Soc. Am.*, *59*, 973–1008.

Karki, B. B., L. Stixrude, and J. Crain (1997), Ab initio elasticity of three high-pressure polymorphs of silica, *Geophys. Res. Lett.*, *24*(24), 3269–3272, doi:10.1029/97GL53196.

Kawakatsu, H., and F. Niu (1994), Seismic evidence for a 920-km discontinuity, *Nature*, *371*, 301–305, doi:10.1038/371301a0.

Kennett, B. L. N., and E. R. Engdahl (1991), Travel times for global earthquake location and phase identification, *Geophys. J. Int.*, *105*, 429–465, doi:10.1111/j.1365-246X.1991.tb06724.x.

Kesson, S. E., J. D. Fitzgerald, and M. G. Shelley (2002), Mineral chemistry and density of subducted basaltic crust at lower-mantle pressures, *Nature*, *372*, 767–769, doi:10.1038/372767a0.

Kingma, K. J., R. E. Cohen, R. J. Hemley, and H. Mao (1995), Transformation of stishovite to a denser phase at lower-mantle pressures, *Nature*, *374*, 243–245, doi:10.1038/374243a0.

Lakshtanov, D. L., et al. (2007), The post-stishovite phase transition in hydrous alumina-bearing SiO_2 in the lower mantle of the Earth, *Proc. Natl. Acad. Sci. U. S. A.*, *104*(34), 13,588–13,590, doi:10.1073/pnas.0706113104.

LeStunff, I., C. W. Wicks, and B. Romanowicz (1995), P'P' precursors under Africa: Evidence for mid-mantle reflectors, *Science*, *270*, 74–77, doi:10.1126/science.270.5233.74.

Muirhead, K. J. (1968), Eliminating false alarms when detecting seismic events automatically, *Nature*, *217*, 533–534, doi:10.1038/217533a0.

Murakami, M., K. Hirose, N. Sata, and Y. Ohishi (2005), Post-perovskite phase transition and mineral chemistry in the pyrolitic lowermost mantle, *Geophys. Res. Lett.*, *32*, L03304, doi:10.1029/2004GL021956.

Niu, F., and H. Kawakatsu (1997), Depth variation of the mid-mantle discontinuity, *Geophys. Res. Lett.*, *24*, 429–432, doi:10.1029/97GL00216.

Nomura, R., K. Hirose, N. Sata, and Y. Ohishi (2010), Precise determination of post-stishovite phase transition boundary and implications for seismic heterogeneities in the mid-lower mantle, *Phys. Earth Planet. Inter.*, doi:10.1016/j.pepi.2010.08.004, in press.

Ono, S., Y. Ohishi, M. Isshiki, and T. Watanuki (2005), In situ X-ray observations of phase assemblages in peridotite and basalt compositions at lower mantle conditions: Implications for density of subducted oceanic plate, *J. Geophys. Res.*, *110*, B02208, doi:10.1029/2004JB003196.

Shen, Y., C. J. Wolfe, and S. C. Solomon (2003), Seismological evidence for a mid-mantle discontinuity beneath Hawaii and Iceland, *Earth Planet. Sci. Lett.*, *214*(1–2), 143–151, doi:10.1016/S0012-821X(03)00349-2.

Tsuchida, Y., and T. Yagi (1989), A new, post-stishovite high pressure polymorph of silica, *Nature*, *340*, 217–220, doi:10.1038/340217a0.

Tsuchiya, T., R. Caracas, and J. Tsuchiya (2004), First principles determination of the phase boundaries of high-pressure polymorphs of silica, *Geophys. Res. Lett.*, *31*, L11610, doi:10.1029/2004GL019649.

Vanacore, E., F. Niu, and H. Kawakatsu (2006), Observations of the mid-mantle discontinuity beneath Indonesia from S to P converted waveforms, *Geophys. Res. Lett.*, *33*, L04302, doi:10.1029/2005GL025106.

Vinnik, L. P., and A. V. Nikolayev (1970), The velocity profile of the lower mantle from direct measurements of $dt/d\Delta$, *Phys. Solid Earth*, *11*, 699–708.

Vinnik, L., F. Niu, and H. Kawakatsu (1998), Broadband converted phases from midmantle discontinuities, *Earth Planets Space*, *50*, 987–997.

Vinnik, L., M. Kato, and H. Kawakatsu (2001), Search for seismic discontinuities in the lower mantle, *Geophys. J. Int.*, *147*, 41–56, doi:10.1046/j.1365-246X.2001.00516.x.

Vinnik, L., S. Oreshin, G. Kosarev, S. Kiselev, and L. Makeyeva (2009), Mantle anomalies beneath southern Africa: Evidence from seismic S

and P receiver functions, *Geophys. J. Int.*, *179*, 279–298, doi:10.1111/j.1365-246X.2009.04261.x.

Wicks, C. W., and M. A. Richards (1993), Seismic evidence for 1200 km discontinuity, *Eos Trans. AGU*, *76*, 329.

Wiechert, E., and K. Zoeppritz (1907), Über Erdbebenwellen, *Nachr. Kgl. Ges. Wiss. Gottingen Math. Phys. Klasse*, *4*, 415–549.

S. I. Oreshin and L. P. Vinnik, Institute of Physics of the Earth, B. Grouzinskaya 10, Moscow 123995, Russia. (vinnik@ifz.ru)

S. Speziale and M. Weber, Deutsches GeoForschungsZentrum, Telegrafenberg, D-14473 Potsdam, Germany.